https://doi.org/10.5194/egusphere-2026-5314
Preprint. Discussion started: 28 September 2026


# Phase-resolved molecular signatures associated with black carbon across biomass fuels and ignition temperatures

Xiaocong Peng[1,#], Wei Song[1,2,3,#], Guohua Zhang[1,2,3,*], Qinhao Lin[4], Jianlin Cheng[1,5], Yang Li[1,5], Xinru Huang[1], Baoyi Chen[1,5], Jianzhong Song[1,2,3], Yingjun Chen[6], Gan Zhang[1,2,3], Ping'an Peng[1,2,3], Xinming Wang[1,2,3], Xinhui Bi[1,2,3]

[1] State Key Laboratory of Environmental Technology, Guangzhou Institute of Geochemistry, Chinese Academy of Sciences (CAS), Guangzhou 510640, PR China

[2] Guangdong Provincial Key Laboratory of Environmental Protection and Resources Utilization, Guangzhou Institute of Geochemistry, CAS, Guangzhou 510640, PR China

[3] Guangdong-Hong Kong-Macao Joint Laboratory for Environmental Pollution and Control, Guangzhou Institute of Geochemistry, CAS, Guangzhou 510640, PR China

[4] School of Environmental Science and Engineering, Institute of Environmental Health and Pollution Control, Guangdong University of Technology, Guangzhou 510006, PR China

[5] University of Chinese Academy of Sciences, Beijing 100049, PR China

[6] Shanghai Key Laboratory of Atmospheric Particle Pollution and Prevention, Department of Environmental Science and Engineering, Fudan University, Shanghai 200438, PR China

#These authors contributed equally to this work.

**Corresponding to* Guohua Zhang (zhanggh@gig.ac.cn)

**Abstract.** Biomass combustion is an important source of black carbon (BC), yet the phase-resolved molecular patterns accompanying black-carbon evolution remain poorly constrained. In particular, detectable molecular signal abundance may not track black-carbon concentration across combustion conditions. Here, we investigated how detectable molecular profiles covary with BC by combining real-time measurements from a proton transfer reaction time-of-flight mass spectrometer (PTR-TOF-MS), for both gas-phase and particle-associated organics, with simultaneous aethalometer (AE-33) BC readings. Experiments were conducted across two biomass fuels (wheat straw and poplar wood) and three ignition temperatures (300, 500, and 700 °C). More than 200 retained nominal-m/z features were classified, and a prespecified block-level screen selected four BC-associated marker families, including furan-ring fragments, oxygenated aromatic, single-ring aromatic (SRA), and polycyclic aromatic hydrocarbons (PAHs), represented by 12 molecular markers. Particle-associated family signals show stronger within-event associations with BC (median block-level Spearman $\rho$ = 0.86–0.92) than corresponding gas-phase signals. Particle-phase molecular profiles improve out-of-experiment BC prediction, increasing $R^2$ from 0.29 to 0.56 beyond a baseline model containing fuel, ignition temperature, and modified combustion efficiency. However, increasing ignition temperature enhanced BC production without a proportional increase in detectable BC-linked marker abundance, indicating a temperature-driven shift from precursor accumulation toward a more conversion-dominated regime. The molecular changes accompanying BC enhancement were fuel-specific, reflecting distinct marker compositions. These findings suggest that biomass BC formation is influenced not simply by detectable marker signal, but by temperature-dependent transformation of fuel-specific molecular pools, providing new constraints for interpreting molecular precursors in biomass-derived BC formation.

https://doi.org/10.5194/egusphere-2026-5314
Preprint. Discussion started: 28 September 2026


**Graphic Abstract**

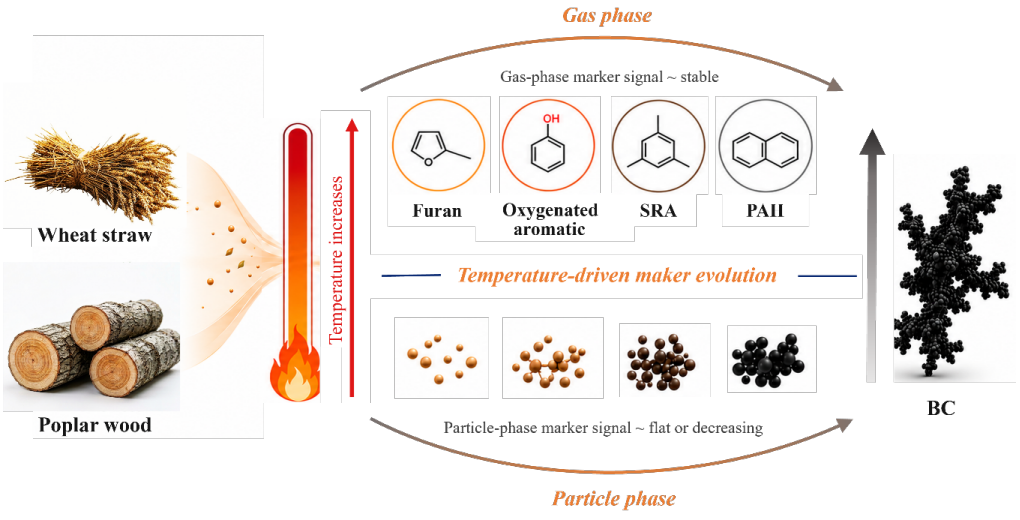

https://doi.org/10.5194/egusphere-2026-5314
Preprint. Discussion started: 28 September 2026


## 1. Introduction

Black carbon (BC) is a key component of fine particulate matter with well-documented impacts on climate forcing, visibility degradation, and public health (Janssen et al., 2011; Bond et al., 2013; IPCC, 2021). Among its global sources, biomass combustion, including agricultural residue burning and residential biofuel use, represents one of the largest and most variable contributors (Bond et al., 2013; Gustafsson et al., 2026). Despite decades of research, the molecular-level processes that govern BC formation from such chemically heterogeneous fuels remain poorly constrained. Reducing BC emissions from biomass burning thus requires not only improved emission inventories but also a mechanistic understanding of how fuel-derived molecular emissions evolve into BC under different combustion conditions.

Our current mechanistic understanding of BC formation is largely derived from high-temperature flame studies using simple gaseous or liquid fuels. In these systems, soot BC formation is commonly described through gas-phase aromatic growth and radical-mediated inception pathways, including hydrogen-abstraction–carbon-addition (HACA), phenyl-addition/cyclization (PAC), resonance-stabilized radical (RSR) chemistry, and subsequent polycyclic aromatic hydrocarbon (PAH) growth, clustering, surface growth, and aggregation (Wang, 2011; Atiku et al., 2017; Johansson et al., 2018; Hussain et al., 2024). Recent studies have further revealed the importance of resonance-stabilized radicals and molecular clustering during soot inception (Wang et al., 2025). However, whether these frameworks fully describe the complex molecular evolution occurring during biomass combustion remains unclear.

Biomass fuels introduce additional complexity because their cellulose-, hemicellulose-, and lignin-derived components generate diverse oxygenated, aromatic, and PAHs during thermal decomposition (Smith et al., 2020; Zhu et al., 2022; Wang et al., 2023; Zhao et al., 2024; Li et al., 2025; Sun et al., 2026). Both low-maturity char-associated BC and high-maturity soot-like BC can form during biomass combustion, and their relative contributions vary with fuel type, ignition temperature, and combustion stage (Han et al., 2021, 2022). Although previous studies have emphasized aromatic precursor formation and PAH growth pathways (Frenklach, 2002; Johansson et al., 2016), it remains unclear whether enhanced BC production primarily reflects increased precursor availability or more efficient transformation of existing molecular pools. Moreover, biomass combustion simultaneously produces gas-phase intermediates and condensed-phase organic materials (Heringa et al., 2012; Li et al., 2025), yet the relative roles of these molecular pools in BC formation remain poorly constrained. A phase-resolved and fuel-specific molecular framework is therefore needed to determine how combustion conditions reorganize molecular signatures associated with BC formation.

Here, we combined phase-resolved PTR-TOF-MS measurements with simultaneous BC observations to establish a phase-resolved molecular framework for investigating biomass BC formation across fuel type and ignition temperature. Specifically, we attempt to address three questions: (1) which molecular families in gas and particle phases are most consistently associated with BC evolution; (2) whether detectable marker signals scale with the BC temperature response; and (3) whether these molecular patterns differ between straw and wood. By linking molecular composition with BC production across phases, fuels, and temperatures, this study provides new constraints on the transformation processes influencing the biomass-derived BC formation.

https://doi.org/10.5194/egusphere-2026-5314
Preprint. Discussion started: 28 September 2026


## 2. Materials and methods

### 2.1 Experimental setup

Combustion experiments were conducted using a laboratory-scale combustion system, including a controlled commercial tube furnace (SK-G06123K-HS, Tianjin Zhonghuan Furnace Co., Ltd., China) and dilution device. Four datasets were collected by batch combustion of wheat straw and poplar wood (two biomass fuels widely used for residential heating and cooking), covering two fuel types × two phases (gas and particle) × three ignition temperatures (300, 500, and 700 °C), which span the smoldering-to-flaming transition (Cui et al., 2023; Zhang et al., 2026). Each temperature segment lasted 30–45 min with 1-min resolution, yielding approximately 25 valid time points per condition-temperature stratum and > 500 time-resolved measurements in total.

The furnace chamber has a diameter of 60 mm and a total length of 1000 mm. Approximately 1–2 g of biomass was loaded into the ignition zone once the furnace reached the target temperature, and combusted for 20–30 min. The generated flue gas was diluted ~50-fold with clean compressed air via a dilution channel sampler to simulate actual flue gas emission conditions, then passed through a buffer tank for thorough mixing and cooling before being directed to downstream instruments.

Real-time analysis was performed using a proton transfer reaction mass spectrometer (PTR-TOF-MS, Model 2000; Ionicon Analytik GmbH, Austria) and an aethalometer (AE33, Magee Scientific). The modified combustion efficiency (MCE) was calculated as $MCE = \Delta CO_2/(\Delta CO + \Delta CO_2)$ based on simultaneous CO and $CO_2$ measurements to characterize the combustion phase (Christian et al., 2003). Prior to each experiment, instruments were calibrated and the system was purged with clean air for at least 1 h to remove residual flue gas and ensure low background levels (BC < 100 ng $m^{-3}$, CO < 0.2 ppm, $CO_2$ < 170 ppm). Most combustion conditions were tested in duplicate, and the variation trends of pollutants at a given temperature were consistent across replicates, confirming the reproducibility of the experimental setup.

### 2.2 VOCs and BC measurements

Gas-phase VOCs and organic signals thermally desorbed from sampled particles were measured by PTR-TOF-MS and a Chemical Analysis of Aerosol On-line (CHARON)–PTR-TOF-MS, respectively, with $H_3O^+$ as the reagent ion. The instrument was operated at a drift tube pressure of 2.5 mbar, drift voltage of 600 V, and temperature of 80 °C, resulting in an E/N ratio of approximately 140 Td. Mass spectra were recorded in the range m/z 15-300 with a time resolution of 1 Hz. Prior to the experiments, calibration of the instrument is conducted using a Compendium Method TO-15 mixed standard gas, which involves zero-air generation and dilution of the standard gas. The gas mixture contains 65 components, including propene, acrolein, acetone, benzene, toluene, 1,2,4-trichlorobenzene, among others (Zhang et al., 2025). Due to the chemical complexity of VOCs from biomass burning, complete calibration of all species was not feasible in our experiments. Nevertheless, the relative transmission efficiencies of $H_3O^+$ and $MH^+$ ions (M = organic compound) through the drift tube and mass spectrometer were estimated from transmission efficiency curves. Before each experiment, mass calibration was performed with $H_3O^+$ (m/z 21.0223) and $CH_3COCH_4^+$ (m/z 59.0490). The observed m/z drifts were minimal, confirming that the mass calibration was adequate for all target compounds (Bruns et al., 2016; Sheng et al., 2018). The raw PTR signals were converted to concentrations (ppb)

https://doi.org/10.5194/egusphere-2026-5314
Preprint. Discussion started: 28 September 2026


based on the reaction rate constant (k) of each compound in the drift tube (Cappellin et al., 2012). For the remaining unassigned ions, a default k value of $2\times10^{-9}$ $cm^3$ $s^{-1}$ was adopted following previous studies (Bruns et al., 2016; Hartikainen et al., 2018). To focus on chemically interpretable organic markers, ions below m/z 40 were excluded. The detailed configuration and connection of the CHARON system have been described previously (Eichler et al., 2015). Briefly, the flue gas was drawn through a filter equipped with an activated-carbon denuder, which removed gaseous organic compounds without affecting the particle mass. Subsequently, an aerodynamic lens was employed to enrich the particle concentration in the PTR-TOF-MS sample flow by approximately 25.6-fold, and the subsample flow was then heated to approximately 160 °C to thermally desorb detectable particulate organics (Eichler et al., 2015; Müller et al., 2017).

Overall, > 200 VOC species were identified and mapped to eight broad chemical classes based on molecular structure and functional groups: N-containing compounds, furan-ring fragments, hydrocarbons (CxHy), carbonyls (including acids and esters), SRA, PAHs, oxygenated aromatics, O-containing compounds, and Others. It is noted that PTR-TOF-MS cannot distinguish isomers, and some m/z values may have multiple contributions.

Particle-phase BC was measured using a seven-wavelength aethalometer operating at 370, 470, 520, 590, 660, 880, and 950 nm, with real-time loading compensation. The instrument uses the dual-spot technique to compensate for filter loading effects. BC mass concentrations were determined at 880 nm using a mass absorption cross-section (MAC) of 7.77 $m^2$ $g^{-1}$ (Petzold et al., 2013), with time resolution set to 1 min. Prior to each experiment, zero checks and flow rate calibrations were performed to ensure proper instrument performance. The detection limit of the AE-33 was ~ 1 ng $m^{-3}$. In addition, gas analyzers for CO (Model 48i, Thermo Scientific, USA) and $CO_2$ (Model 410i, Thermo Scientific, USA) were employed to monitor the concentration changes of relevant gases during biomass burning in real time.

### 2.3 Statistical workflow

The statistical framework was designed to resolve species-level VOC–BC associations while accounting for the hierarchical structure of the experimental design. The primary analytical unit is an event block, defined as a unique combination of fuel, sampling phase, replicate experiment, and ignition temperature, resulting in 21 valid blocks across the four fuel–phase combinations and three ignition temperatures. Within each block, Spearman rank correlations (ρ) were computed between each VOC species and BC across ~25 time points, then aggregated across blocks using median values to obtain cross-condition associations.

To identify core BC-associated marker families, we applied the selection criteria: (i) median $|\rho| \geq 0.7$ across blocks, (ii) representation by at least two species within a chemical class. Marker selection was then conducted only within the retained core families. More detail for the classification and the sensitivity test can be found in Text S1. Temperature-normalized responses were computed by normalizing median signals at each temperature to the 300 °C baseline. The BC-marker ratio is defined as log(BC/Σcore marker signal), serving as an operational metric of BC production efficiency relative to detectable marker abundance.

To independently assess whether phase-resolved molecular profiles contained BC-relevant information beyond ignition temperature, fuel type, and MCE, we fitted Ridge regression models and evaluated them using nested leave-

https://doi.org/10.5194/egusphere-2026-5314
Preprint. Discussion started: 28 September 2026


one-experiment-out cross-validation. BC concentrations were natural-log transformed before model fitting because their distributions are strongly right-skewed and showed increasing variance at higher concentration levels. The response variable is ln(BC), and the baseline model included ignition temperature, fuel identity, and MCE. Molecular models additionally included total VOC signal, broad chemical-class signals, the core BC-associated marker families, the selected markers, or all annotated ions. In each outer validation fold, all observations from one combustion experiment were withheld from model fitting and used exclusively for external evaluation. Partial least-squares regression was used as an independent sensitivity analysis. A within-block circular-shift permutation test was further performed to assess whether the predictive improvement depended on the temporal alignment between molecular profiles and BC. Detailed model specifications and sensitivity analyses are provided in Text S2.

## 3. Results and discussion

### 3.1 Temperature responses of BC and molecular composition

Figure 1 provides an integrated overview of BC emissions and concurrent VOC compositions across the four experimental conditions from 300 to 700 °C. It can be seen that BC concentrations increase with ignition temperature across both biomass fuels, with median values rising from 209–430 ng $m^{-3}$ at 300 °C to 818–896 ng $m^{-3}$ at 700 °C. The distributions become increasingly right-skewed at 700 °C, particularly in Wood-Gas (mean = 9, 742 ng $m^{-3}$, median = 818 ng $m^{-3}$) and Straw-Particle (mean = 6, 910 ng $m^{-3}$, median = 896 ng $m^{-3}$), indicating enhanced variability under high-temperature combustion conditions. These observations are consistent with previous studies showing increased BC emissions and episodic high-emission events during more intense biomass combustion conditions (Han et al., 2021, 2022).

https://doi.org/10.5194/egusphere-2026-5314
Preprint. Discussion started: 28 September 2026


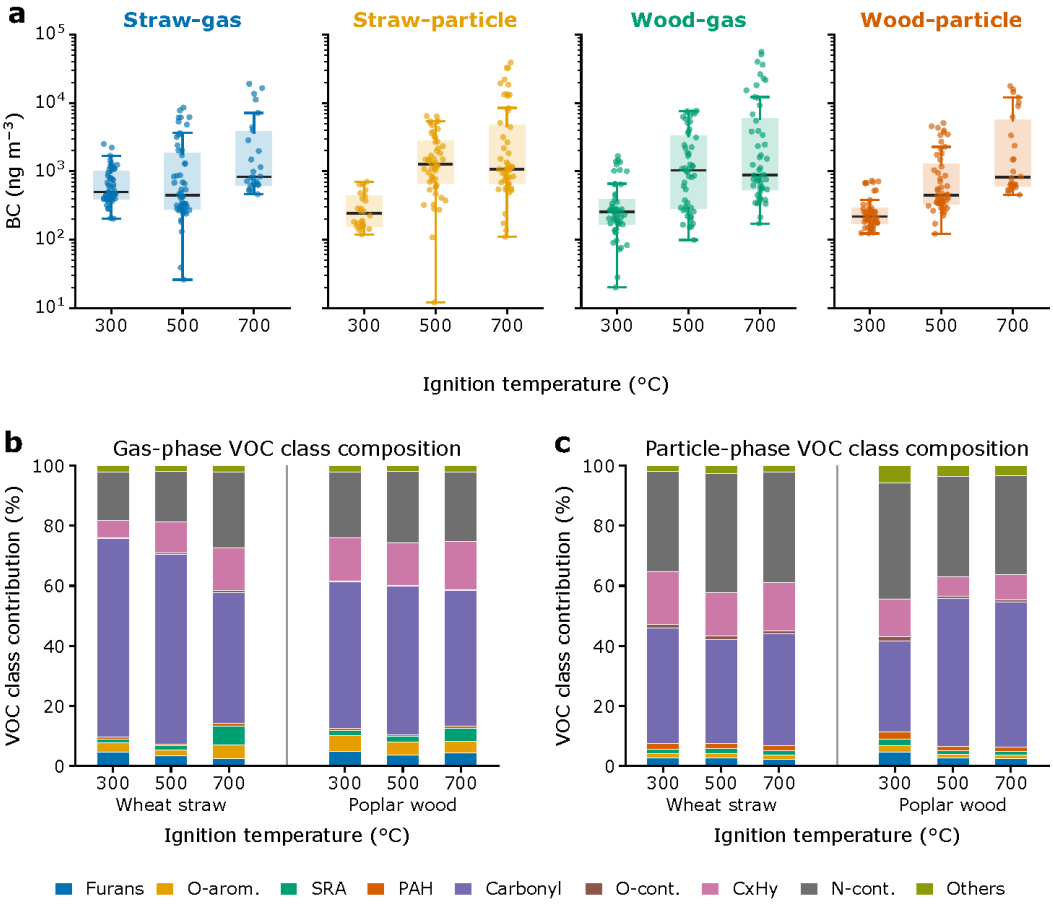


**Figure 1. Temperature responses of BC and VOC class composition across fuel type and sampling phase. (a) Distributions of BC concentrations for wheat straw and poplar wood in gas- and particle-phase experiments at ignition temperatures of 300, 500, and 700 °C. Boxes indicate the interquartile range, center lines indicate medians, whiskers indicate 1.5× the interquartile range, and points represent individual time-resolved observations. Relative contributions of VOC broad classes in the (b) gas phase and (c) particle phase.**

In contrast to the monotonic increase in BC, total VOC signals show non-monotonic temperature responses (Figure S1), suggesting that BC enhancement is not simply accompanied by greater detectable organic emissions. Instead, ignition temperature strongly changes the molecular composition. As shown in Figure 1b, the overall distribution of the broad-class VOCs (including > 200 detected species) is consistent with previous biomass-burning observations, in which aromatic hydrocarbons, phenolic compounds, and furan-ring fragments are among many important compound classes (Stockwell et al., 2015). In the gas phase, carbonyl compounds dominated across all conditions (45-67% of cumulative signal), followed by N-containing species (14-23%) and CxHy hydrocarbons (8-16%). The carbonyl fraction decreases with increasing temperature (67% at 300 °C to 45% at 700 °C for straw), while N-containing and SRA fractions increase, reflecting progressive thermal decomposition of nitrogenous biomass components and aromatization at higher temperatures. For example, Wood-Gas maintains relatively stable total VOC

https://doi.org/10.5194/egusphere-2026-5314
Preprint. Discussion started: 28 September 2026


signals across temperatures while the SRA fraction increases approximately six-fold from 300 to 700 °C, suggesting substantial compositional restructuring rather than simple emission enhancement. This trend is consistent with temperature-driven decomposition and deoxygenation of lignin-derived oxygenated compounds, leading to enrichment of less oxygenated aromatic species at higher temperatures (Zhu et al., 2022).

The particle phase exhibits a distinct molecular composition compared with the gas phase. Carbonyl compounds remained abundant (32-50%), while N-containing compounds represents a larger fraction (30-36%), particularly for straw combustion. Furans-related signals account for 2-5% of particle-phase molecular abundance, with slightly higher contributions in wood than straw. These phase-dependent differences indicate that thermal conditions regulate not only the total abundance but also the molecular organization of condensed organic material associated with BC formation.

### 3.2 Phase-resolved BC-associated molecular families and markers

The monotonic increase in BC with temperature, contrasting with the non-monotonic trends of VOC signals, reflects that BC formation is not uniformly linked to all VOC classes. Instead, reproducible event-profile coupling is concentrated in a subset of biomass-derived molecular families. Four of these classes were identified as core BC-associated marker families: furan-ring fragments, oxygenated aromatic, SRA, and PAH (Fig. 2a and Table S1). Rather than representing independent precursors, these molecular families represent particle-phase compositional states associated with BC evolution. The same four-family marker set is retained across the tested threshold grid (Text S1). O-containing and CxHy classes also show high coupling in some summaries, but no marker species meet the same coverage criteria; their effective block coverage was lower (13 blocks; Table S1).

The phase-resolved analysis further shows that particle-phase molecular profiles provide a stronger BC-relevant signal than gas-phase VOC profiles. Across the four core families, median particle-phase Spearman correlations ($\rho$ = 0.86–0.92) with BC are uniformly high and stable, whereas gas-phase correlations are weaker and, for SRA and PAH markers, close to zero or negative in the median summary (Figure 2a). The particularly weak gas-phase associations of SRA and PAH indicate that their BC-relevant information is expressed primarily in particle-associated profiles. This pattern may arise from several nonexclusive processes, including shared combustion-stage dependence, gas–particle partitioning, transformation of semi-volatile material, and incorporation of oxygenated or aromatic species into BC-containing particles.

https://doi.org/10.5194/egusphere-2026-5314
Preprint. Discussion started: 28 September 2026


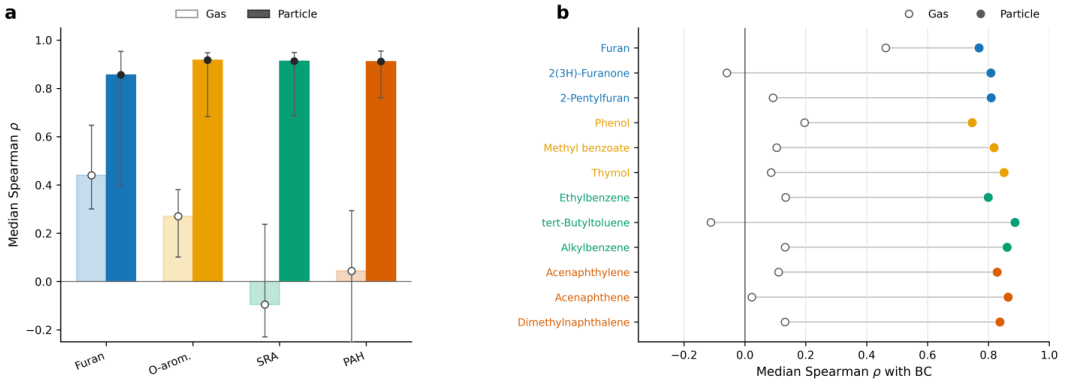


**Figure 2. Phase-resolved molecular associations with BC. (a) Gas- and particle-phase median coupling for the four selected core families. Error bars show bootstrap intervals across available blocks. (b) Gas- and particle-phase median block correlations for the 12 representative markers selected by the rules in Tables S1-S2.**

Gas-phase molecular composition nevertheless changes substantially with ignition temperature. For straw, the furans-related signals contribution to the four-family gas-phase pool decreases from ~60% at 300 °C to ~20% at 700 °C, while the SRA fraction increases from ~10% to ~40% (Figure S2). Wood shows a weaker but similar redistribution: furans-related signals decreases from ~40% to ~10% and SRA increases from ~15% to ~35%. These shifts are broadly consistent with previous biomass studies reporting a temperature-dependent redistribution from oxygenated products toward more aromatic products, including increased PAH contributions at elevated temperatures (Zhu et al., 2022; Zhao et al., 2024; Li et al., 2025) . In particle-phase emissions, the four core families together account for 6.8–12.9% of the total retained molecular signal. Although they represent only a limited fraction of the detected particle-phase composition, their relative contributions are highly structured: furans-related signals is consistently the largest component, accounting for 28–42% of the core-family pool across conditions (Figure S3). The prominence of furans-related signals is qualitatively consistent with flame studies reporting furanic and other oxygenated functionalities in incipient soot, although direct comparison should be made cautiously because those studies examined controlled hydrocarbon flames rather than biomass combustion (Johansson et al., 2016) .

To determine whether these family-level associations are supported by individual molecular features, three representative markers are selected from each core family based on complete block coverage, consistent particle-phase BC coupling, and relative signal abundance (Table S2 and Figure S4). Their median particle-phase correlations with BC range from 0.75 to 0.89, whereas the corresponding gas-phase correlations are weaker and more variable, ranging from −0.11 to 0.46 (Figure 2b). The coherence of particle-phase coupling at both the family level and the individual-marker level supports the use of these features as a reproducible, phase-specific marker representation of within-event BC variation. Ridge regression shows that the addition of the four core-family signals increase the leave-one-experiment-out $R^2$ from 0.29 to 0.56 for particle-phase data and reduces the log-scale mean absolute error from 0.86 to 0.65 (Figure S5). In contrast, adding the same molecular representation does not improve gas-phase prediction. These results indicate that the four particle-phase core families contain reproducible information on BC-associated event evolution beyond that provided by temperature, fuel type, and MCE.

https://doi.org/10.5194/egusphere-2026-5314
Preprint. Discussion started: 28 September 2026


### 3.3 Temperature-dependent marker-BC divergence

The normalized response analysis reveals a clear divergence between BC concentration and summed detectable core-marker signal along the ignition-temperature gradient. Across fuel–phase conditions, BC increases much more strongly than the summed core marker signal from 300 to 700 °C (Figure 3a). This divergence is most evident in the particle phase. For straw particles, median BC increases by more than fourfold from 300 to 700 °C, whereas the summed particle-phase core marker signal remains close to its 300 °C level. For wood particles, BC increases progressively with temperature, while the detectable core marker pool declines. Gas-phase profiles exhibit more fuel-dependent behavior: straw gas-phase core markers partially recover at 700 °C, whereas wood gas-phase core markers remain below their 300 °C level. Therefore, elevated ignition temperature does not simply expand the detectable pool of BC-linked molecular markers; rather, it alters the relationship between detectable marker signal and BC formation.

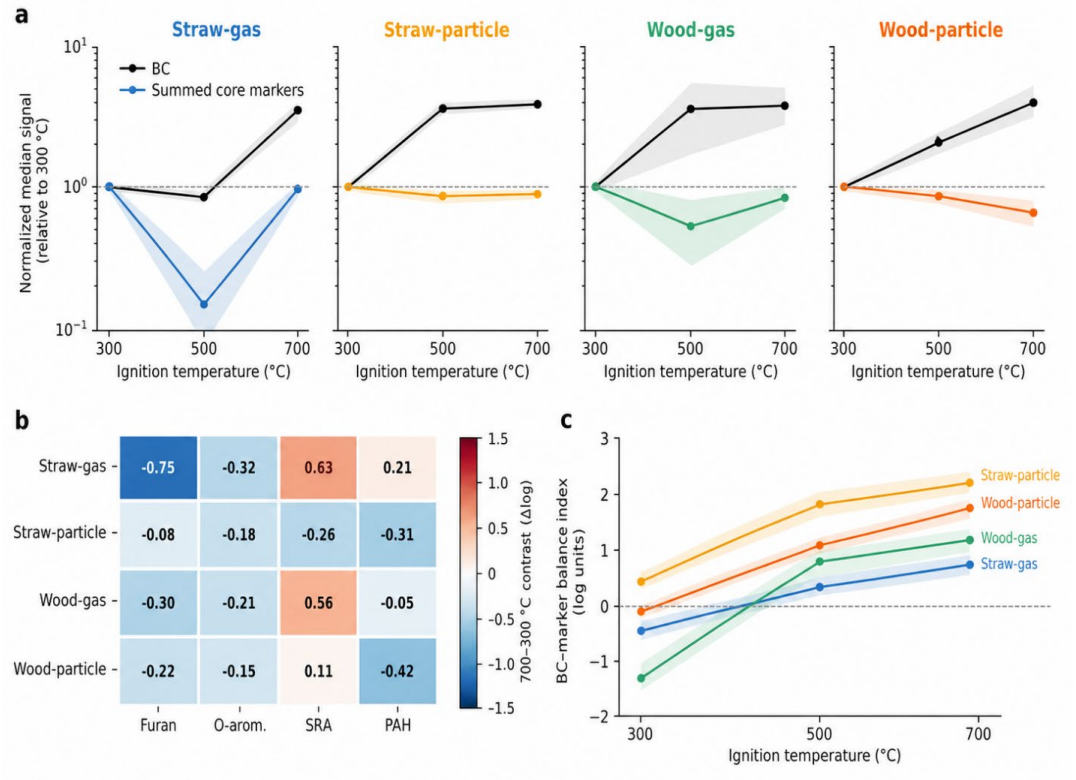


**Figure 3. Divergence between detectable core-marker signal and BC concentration across ignition temperature. (a) Temperature-normalized responses of BC and summed core marker signals across fuel–phase conditions. Values are normalized to the corresponding 300 °C median for each condition. (b) Paired 700–300 °C contrasts for individual core marker families. (c) Temperature dependence of the BC-marker ratio.**

The class-specific 700–300 °C contrasts further show that this decoupling is distributed across multiple molecular families rather than being driven by a single class (Figure 3b). BC increases strongly across all fuel–phase conditions, with positive Δlog BC values, whereas total core marker detectable signal abundance changes weakly or declines.

https://doi.org/10.5194/egusphere-2026-5314
Preprint. Discussion started: 28 September 2026


Furans and oxygenated-aromatic signal abundance generally decreases or fails to increase with temperature, especially in the particle phase. The concurrent depletion of detectable furans-related markers and enrichment of SRA signals observed here is therefore consistent with enhanced aromatic-growth chemistry, although direct conversion of furans-derived carbon into BC was not established. Previous studies indicate that furans compounds can undergo ring-opening and fragmentation pathways that generate small unsaturated species and resonance-stabilized radicals, which subsequently contribute to the formation of benzene, substituted monoaromatics, and larger PAHs (Tran et al., 2015; Cheng et al., 2017). PAH markers, in contrast, show the weakest temperature response among the four families. This muted behavior suggests two possibilities: PAH growth toward higher molecular weights may occur below the detection threshold of our m/z range, or PAH incorporation into BC particles may be sufficiently rapid to prevent accumulation in either phase.

The BC-marker ratio increases with ignition temperature across all four fuel–phase conditions (Figure 3c), indicating that BC accumulation increasingly outpaced the detectable marker pool. Its increase may reflect faster turnover of molecular intermediates, redistribution between phases, formation of compounds outside the measured m/z range, or incorporation into less volatile carbonaceous material. These processes are broadly consistent with established pathways of aromatic growth and soot-particle evolution, but their relative contributions cannot be resolved by the present measurements (Frenklach, 2002; Zhu et al., 2022; Shao et al., 2023; Li et al., 2025). The observed pattern may also be viewed in light of the distinct char BC and soot-BC formation pathways reported for solid-fuel combustion, whose relative importance varies with fuel composition, combustion temperature, and combustion stage (Han et al., 2022).

This interpretation refines, rather than contradicts, the marker-BC linkage identified in Figure 2. The apparent marker-BC divergence may therefore be interpreted as evidence for a temperature-driven fate shift. In this framework, furans and oxygenated-aromatic markers should not be interpreted simply as soot promoters or inhibitors. Under oxygen-rich or additive-modified conditions, oxygenated species may suppress soot BC by enhancing oxidative fragmentation (Xu et al., 2022; Hussain et al., 2024), whereas in biomass combustion they may also represent oxygen-rich intermediates or particle-associated structures involved in char-like BC formation (Johansson et al., 2016).

### 3.4 Fuel-specific molecular composition and BC-associated diagnostics

Figure 4 examines whether fuel type changes the magnitude of particle-phase BC-associated marker signals. When integrated across ignition temperatures, wood exhibited higher signals than straw for all four core families, but the magnitude of enrichment differed among families (Figure 4a). Furans-related signals shows the strongest wood/straw enrichment, followed by oxygenated aromatics, SRA, and PAHs. The temperature-resolved compositions show a consistent contrast: straw retains a comparatively balanced four-family pool, whereas wood remains more furans-rich and has a smaller relative PAHs contribution across 300–700 °C (Figure 4b). Thus, fuel type does not simply scale a common particle-phase molecular profile; it alters the relative organization of the BC-associated core-family pool. This fuel contrast is chemically plausible given the distinct but overlapping products generated from lignocellulosic components. Thermal decomposition of cellulose, hemicellulose, and lignin produces different mixtures of furans, phenolic, oxygenated-aromatic, and PAHs-related products, whose distributions vary with

https://doi.org/10.5194/egusphere-2026-5314
Preprint. Discussion started: 28 September 2026


temperature and combustion conditions (Zhu et al., 2022; Wang et al., 2023; Romanias et al., 2024; Li et al., 2025). Bulk lignocellulosic composition alone, however, cannot explain the observed particle-phase profiles. Fuel-dependent volatilization, secondary reactions, gas-particle partitioning, and retention of semi-volatile material may also contribute. Because these processes are not resolved separately, our results are best interpreted as evidence of fuel-specific molecular organization rather than direct allocation of cellulose-, hemicellulose-, or lignin-derived carbon.

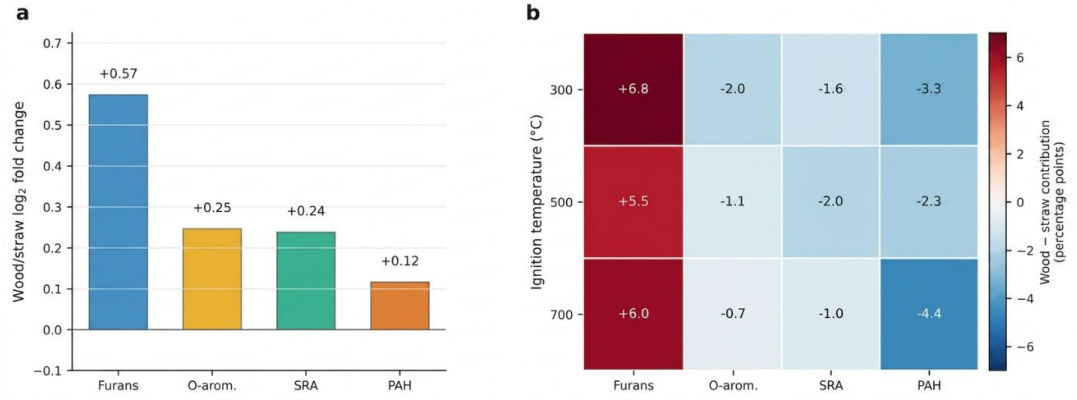


**Figure 4. Fuel-dependent composition of the particle-associated BC-marker pool. (a) Wood/straw $log_2$ fold changes in cumulative particle-phase signal abundance of the four core marker families. (b) Temperature-resolved wood–straw differences in four-family core-pool composition.**

Given this fuel dependence, we next tested whether composition-based diagnostics could nevertheless provide a common indicator of BC enhancement across the two fuels (Figure 5a). None of the evaluated ratios show a strong and consistent relationship with BC in both the pooled and fuel-stratified analyses. The oxygenated-aromatics/furans ratio shows the strongest pooled association and remained positively related to BC in both fuels. Its temperature response is more obvious for wood, for which the ratio increases from 300 to 500 °C and then changes little (Figure 5b). Its increase may result from both the oxygenated-aromatic enrichment and furans depletion as discussed in the above section. It should therefore be interpreted as an empirical measure of compositional redistribution within the core-family pool.

The high-/low-m/z PAH ratio exhibits a different fuel dependence, increasing progressively with temperature in straw but changing little in wood. This pattern indicates redistribution toward higher-m/z features within the detectable PAH pool for straw, but it does not directly demonstrate PAH molecular growth, increasing ring number, or soot maturation. The aromatic-advancement, PAH/oxygenated-pool, and indene/PAH ratios similarly show only moderate pooled associations or inconsistent fuel-specific behavior. Although PAH growth and resonance-stabilized radicals, including indenyl, are mechanistically important in soot-inception studies, ratios derived from detected products do not necessarily track the controlling chemistry of BC formation in complex biomass emissions (Frenklach, 2002). Overall, fuel identity constrains both the molecular expression of BC-associated particle states and the transferability of composition-based diagnostics. The full multivariate molecular profile therefore provides a more robust description of BC-associated variation across fuels than any single diagnostic ratio.

https://doi.org/10.5194/egusphere-2026-5314
Preprint. Discussion started: 28 September 2026


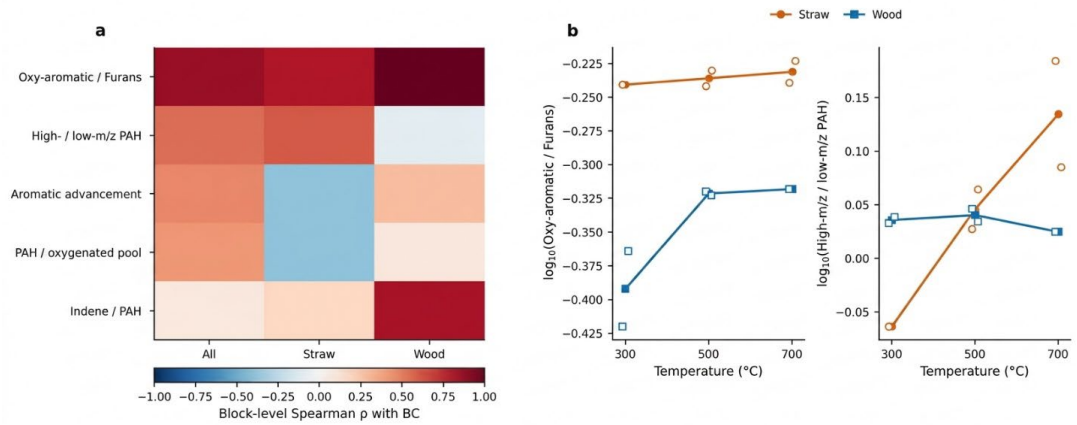


**Figure 5. Fuel-dependent particle-phase molecular diagnostics associated with BC. (a) Block-level Spearman correlations between five mechanistically motivated molecular diagnostics and BC, calculated for all particle-phase blocks and separately for straw and wood combustion. (b) Temperature responses of the two selected diagnostics: $\log_{10}$ (oxygenated aromatics/furans) and $\log_{10}$ (high-m/z PAHs/low-m/z PAHs). High- and low-m/z PAHs were operationally separated at nominal m/z = 179 (ref: 2-3 rings for low MW PAHs; 4-6 rings for high MW PAHs) (Wang et al., 2023).**

## 4. Implications and limitations

This study shows that BC-associated molecular signals during biomass combustion are varied with fuel type, ignition temperature, and sampling phase. Four molecular families display reproducible associations with BC in particle-phase emissions, whereas their gas-phase relationships are weaker and more fuel dependent. Moreover, BC increased more strongly with ignition temperature than the detectable core-marker pool. Together, these results indicate that higher BC production cannot be explained solely by greater abundance of detectable molecular markers. Instead, ignition temperature appears to reorganize the phase distribution and detectable expression of oxygenated and aromatic molecular pools. This interpretation complements classical soot-formation frameworks, which primarily describe aromatic growth, particle inception, and surface growth in high-temperature flames of relatively simple fuels (Frenklach, 2002; Wang, 2011; Altarawneh and Ali, 2024). The present results extend this perspective to chemically heterogeneous biomass combustion by identifying fuel- and phase-dependent molecular states associated with BC evolution, while not resolving the underlying reaction pathways directly.

These molecular observations may also help explain the large variability in biomass-burning BC emission factors. Current inventories generally classify emissions according to fuel type and combustion characteristics, but the molecular processes underlying variations within these categories remain poorly constrained (Andreae and Merlet, 2001; Akagi et al., 2011; Van Der Werf et al., 2017) . The observed separation between BC accumulation and detectable marker abundance provides a potential molecular basis for nonlinear BC responses to changing combustion conditions. However, the present experiments were not designed to derive fuel-normalized emission factors or inventory-ready parameterizations. Translating the observed relationships into atmospheric models will require coordinated measurements of fuel consumption, BC emission factors, combustion efficiency, and phase-resolved molecular composition across continuous temperature and oxygen gradients and a wider range of fuels.

https://doi.org/10.5194/egusphere-2026-5314
Preprint. Discussion started: 28 September 2026


Several constraints of the present study should be acknowledged. First, molecular assignments are based on nominal-m/z PTR-TOF-MS annotations and therefore include structural and isomeric ambiguity; the identified species should be interpreted as representative markers of broader molecular families rather than uniquely resolved compounds. Second, the detectable marker pool represents only part of the molecular material associated with BC formation. The m/z range (40–300) does not capture high-molecular-weight PAHs and non-volatile oligomeric species that may contribute to particle inception and growth. Third, the analysis is based on observational event-profile coupling across a finite number of experimental blocks in a laboratory tube furnace, which provides controlled and reproducible conditions but does not fully replicate the temperature gradients, oxygen variability, and fuel heterogeneity of open or residential biomass burning.

https://doi.org/10.5194/egusphere-2026-5314
Preprint. Discussion started: 28 September 2026


## Data availability

The data used in this study are available from the corresponding authors upon request: Guohua Zhang (zhanggh@gig.ac.cn).

## Supplement

Supporting information includes two texts (Text S1-S2), two tables (Table S1-S2), and Five figures (Fig. S1-S5) related to the manuscript.

## Author contribution

GuohZ designed and conceptualized the research. XP, CJ, YL, XH and BC conducted the measurements. WS XW and QL provided support for instruments and instructions of the experiment. XP and GuohZ analyzed the data. JS, YC, GZ, PP, XW and XB reviewed and commented on the paper. XP, WS and GuohZ wrote and edited the paper.

## Competing interests

The authors declare that they have no known competing financial interests.

## Financial support

This work was funded by the National Natural Science Foundation of China (42192514 and 42577110) and Guangdong Foundation for Program of Science and Technology Research (2023B0303000007).

## References

Akagi, S. K., Yokelson, R. J., Wiedinmyer, C., Alvarado, M. J., Reid, J. S., Karl, T., Crounse, J. D., and Wennberg, P. O.: Emission factors for open and domestic biomass burning for use in atmospheric models, Atmos. Chem. Phys., 11, 4039-4072, 10.5194/acp-11-4039-2011, 2011.

Altarawneh, M. and Ali, L.: Formation of Polycyclic Aromatic Hydrocarbons (PAHs) in Thermal Systems: A Comprehensive Mechanistic Review, Energy & Fuels, 38, 21735-21792, 10.1021/acs.energyfuels.4c03513, 2024.

Andreae, M. O. and Merlet, P.: Emission of trace gases and aerosols from biomass burning, Global Biogeochemical Cycles, 15, 955-966, 10.1029/2000gb001382, 2001.

Atiku, F. A., Lea-Langton, A. R., Bartle, K. D., Jones, J. M., Williams, A., Burns, I. S., and Humphries, G. S.: Some Aspects of the Mechanism of Formation of Smoke from the Combustion of Wood, Energy & Fuels, 31, 1935-1944, 10.1021/acs.energyfuels.6b02639, 2017.

https://doi.org/10.5194/egusphere-2026-5314
Preprint. Discussion started: 28 September 2026


380 Bond, T. C., Doherty, S. J., Fahey, D. W., Forster, P. M., Berntsen, T., DeAngelo, B. J., Flanner, M. G., Ghan, S., Karcher, B., Koch, D., Kinne, S., Kondo, Y., Quinn, P. K., Sarofim, M. C., Schultz, M. G., Schulz, M., Venkataraman, C., Zhang, H., Zhang, S., Bellouin, N., Guttikunda, S. K., Hopke, P. K., Jacobson, M. Z., Kaiser, J. W., Klimont, Z., Lohmann, U., Schwarz, J. P., Shindell, D., Storelvmo, T., Warren, S. G., and Zender, C. S.: Bounding the role of black carbon in the climate system: A scientific assessment, J. Geophys. Res.-Atmos., 118, 5380-5552, 10.1002/jgrd.50171, 385 2013.

Bruns, E. A., El Haddad, I., Slowik, J. G., Kilic, D., Klein, F., Baltensperger, U., and Prévôt, A. S. H.: Identification of significant precursor gases of secondary organic aerosols from residential wood combustion, Scientific Reports, 6, 10.1038/srep27881, 2016.

Cappellin, L., Karl, T., Probst, M., Ismailova, O., Winkler, P. M., Soukoulis, C., Aprea, E., Märk, T. D., Gasperi, F., 390 and Biasioli, F.: On Quantitative Determination of Volatile Organic Compound Concentrations Using Proton Transfer Reaction Time-of-Flight Mass Spectrometry, Environ. Sci. Technol., 46, 2283-2290, 10.1021/es203985t, 2012.

Cheng, Z. J., Tan, Y. Y., Wei, L. X., Xing, L. L., Yang, J. Z., Zhang, L. D., Guan, Y. N., Yan, B. B., Chen, G. Y., and Leung, D. Y. C.: Experimental and kinetic modeling studies of furan pyrolysis: Fuel decomposition and aromatic ring formation, Fuel, 206, 239-247, 10.1016/j.fuel.2017.05.090, 2017.

395 Christian, T. J., Kleiss, B., Yokelson, R. J., Holzinger, R., Crutzen, P. J., Hao, W. M., Saharjo, B. H., and Ward, D. E.: Comprehensive laboratory measurements of biomass-burning emissions: 1. Emissions from Indonesian, African, and other fuels - art. no. 4719, J. Geophys. Res.-Atmos., 108, 10.1029/2003jd003704, 2003.

Cui, M., Xu, Y. Y., Yu, B. B., Yan, C. Q., Li, J., Zheng, M., and Chen, Y. J.: Characterization of carbonaceous matter emitted from residential coal and biomass combustion by experimental simulation, Atmos. Environ., 293, 400 10.1016/j.atmosenv.2022.119447, 2023.

Eichler, P., Müller, M., D'Anna, B., and Wisthaler, A.: A novel inlet system for online chemical analysis of semi-volatile submicron particulate matter, Atmos. Meas. Tech., 8, 1353-1360, 10.5194/amt-8-1353-2015, 2015.

Frenklach, M.: Reaction mechanism of soot formation in flames, Phys. Chem. Chem. Phys., 4, 2028-2037, 10.1039/b110045a, 2002.

405 Gustafsson, Ö., Budhavant, K., Chimurkar, N., Clarke, S., Dreyfus, G., Gong, X., Klimont, Z., Klingmüller, K., Kim, S. W., Lelieveld, J., Myhre, G., Nair, H., Peng, J. F., Ramanathan, V., Rana, A., Manoj, M. R., Satheesh, S. K., Venkataraman, C., and Zhang, Q.: Atmospheric black carbon in the climate system, Nature Reviews Earth & Environment, 7, 312-328, 10.1038/s43017-026-00773-3, 2026.

Han, Y., Chen, Y. J., Feng, Y. L., Shang, Y., Li, J., Li, Q., and Chen, J. M.: Fuel Aromaticity Promotes Low-410 Temperature Nucleation Processes of Elemental Carbon from Biomass and Coal Combustion, Environ. Sci. Technol., 55, 2532-2540, 10.1021/acs.est.0c06694, 2021.

Han, Y., Chen, Y. J., Feng, Y. L., Shang, Y., Li, J., Li, Q., and Chen, J. M.: Existence and Formation Pathways of High- and Low-Maturity Elemental Carbon from Solid Fuel Combustion by a Time-Resolved Study, Environ. Sci. Technol., 56, 2551-2561, 10.1021/acs.est.1c05216, 2022.

415 Hartikainen, A., Yli-Pirilä, P., Tiitta, P., Leskinen, A., Kortelainen, M., Orasche, J., Schnelle-Kreis, J., Lehtinen, K. E. J., Zimmermann, R., Jokiniemi, J., and Sippula, O.: Volatile Organic Compounds from Logwood Combustion:

https://doi.org/10.5194/egusphere-2026-5314
Preprint. Discussion started: 28 September 2026


Emissions and Transformation under Dark and Photochemical Aging Conditions in a Smog Chamber, Environ. Sci. Technol., 52, 4979-4988, 10.1021/acs.est.7b06269, 2018.

Heringa, M. F., DeCarlo, P. F., Chirico, R., Lauber, A., Doberer, A., Good, J., Nussbaumer, T., Keller, A., Burtscher, H., Richard, A., Miljevic, B., Prevot, A. S. H., and Baltensperger, U.: Time-Resolved Characterization of Primary Emissions from Residential Wood Combustion Appliances, Environ. Sci. Technol., 46, 11418-11425, 10.1021/es301654w, 2012.

Hussain, B., Li, W., Fang, Q. L., and Li, Y. Y.: Synergistic Effects of Fuel Components on Aromatics Formation in Combustion: A Review, Applied Sciences-Basel, 14, 10.3390/app14156720, 2024.

IPCC: Climate Change 2021: The Physical Science Basis. Contribution of Working Group I to the Sixth Assessment Report of the Intergovernmental Panel on Climate Change, Cambridge University Press, Cambridge, United Kingdom and New York, NY, USA, 10.1017/9781009157896, 2021.

Janssen, N. A. H., Hoek, G., Simic-Lawson, M., Fischer, P., van Bree, L., ten Brink, H., Keuken, M., Atkinson, R. W., Anderson, H. R., Brunekreef, B., and Cassee, F. R.: Black Carbon as an Additional Indicator of the Adverse Health Effects of Airborne Particles Compared with PM10 and PM2.5, Environ. Health Perspect., 119, 1691-1699, 10.1289/ehp.1003369, 2011.

Johansson, K. O., Head-Gordon, M. P., Schrader, P. E., Wilson, K. R., and Michelsen, H. A.: Resonance-stabilized hydrocarbon-radical chain reactions may explain soot inception and growth, Science, 361, 997-+, 10.1126/science.aat3417, 2018.

Johansson, K. O., Dillstrom, T., Monti, M., El Gabaly, F., Campbell, M. F., Schrader, P. E., Popolan-Vaida, D. M., Richards-Henderson, N. K., Wilson, K. R., Violi, A., and Michelsen, H. A.: Formation and emission of large furans and oxygenated hydrocarbons from flames, Proc. Natl. Acad. Sci. U. S. A., 113, 8374-8379, 10.1073/pnas.1604772113, 2016.

Li, J. S., Xu, K. L., Yao, X. W., and Luo, X. Y.: Investigation into the Multiphase Product Distribution and Evolution During Biomass Pyrolysis Using Wheat Straw and Pine Sawdust, Energies, 18, 10.3390/en18205397, 2025.

Müller, M., Eicher, P., D'Anna, B., Tan, W., and Wisthaler, A.: Direct Sampling and Analysis of Atmospheric Particulate Organic Matter by Proton-Transfer-Reaction Mass Spectrometry, Anal. Chem., 89, 10889-10897, 10.1021/acs.analchem.7b02582, 2017.

Petzold, A., Ogren, J. A., Fiebig, M., Laj, P., Li, S. M., Baltensperger, U., Holzer-Popp, T., Kinne, S., Pappalardo, G., Sugimoto, N., Wehrli, C., Wiedensohler, A., and Zhang, X. Y.: Recommendations for reporting "black carbon" measurements, Atmos. Chem. Phys., 13, 8365-8379, 10.5194/acp-13-8365-2013, 2013.

Romanias, M. N., Coggon, M. M., Al Ali, F., Burkholder, J. B., Dagaut, P., Decker, Z., Warneke, C., Stockwell, C. E., Roberts, J. M., Tomas, A., Houzel, N., Coeur, C., and Brown, S. S.: Emissions and Atmospheric Chemistry of Furanoids from Biomass Burning: Insights from Laboratory to Atmospheric Observations, Acs Earth and Space Chemistry, 8, 857-899, 10.1021/acsearthspacechem.3c00226, 2024.

Shao, C., Wang, Q., Zhang, W., Bennett, A., Li, Y., Guo, J. J., Im, H. G., Roberts, W. L., Violi, A., and Sarathy, S. M.: Elucidating the polycyclic aromatic hydrocarbons involved in soot inception, Communications Chemistry, 6, 10.1038/s42004-023-01017-x, 2023.

https://doi.org/10.5194/egusphere-2026-5314
Preprint. Discussion started: 28 September 2026


Sheng, J. J., Zhao, D. L., Ding, D. P., Li, X., Huang, M. Y., Gao, Y., Quan, J. N., and Zhang, Q.: Characterizing the level, photochemical reactivity, emission, and source contribution of the volatile organic compounds based on PTR-TOF-MS during winter haze period in Beijing, China, Atmos. Res., 212, 54-63, 10.1016/j.atmosres.2018.05.005, 2018.

Smith, D. M., Cui, T. Q., Fiddler, M. N., Pokhrel, R. P., Surratt, J. D., and Bililign, S.: Laboratory studies of fresh and aged biomass burning aerosol emitted from east African biomass fuels - Part 2: Chemical properties and characterization, Atmos. Chem. Phys., 20, 10169-10191, 10.5194/acp-20-10169-2020, 2020.

Stockwell, C. E., Veres, P. R., Williams, J., and Yokelson, R. J.: Characterization of biomass burning emissions from cooking fires, peat, crop residue, and other fuels with high-resolution proton-transfer-reaction time-of-flight mass spectrometry, Atmos. Chem. Phys., 15, 845-865, 10.5194/acp-15-845-2015, 2015.

Sun, H., Wang, J. L., Liu, W., Ruan, L., Yang, Z. M., Ma, X. Q., Chen, X. W., Xu, L., Du, L., Liu, Q. F., and Li, K.: Smoldering of crop residues emits a large amount of intermediate volatility organic compounds to the atmosphere, Journal of Hazardous Materials, 508, 10.1016/j.jhazmat.2026.141877, 2026.

Tran, L. S., Sirjean, B., Glaude, P. A., Kohse-Höinghaus, K., and Battin-Leclerc, F.: Influence of substituted furans on the formation of Polycyclic Aromatic Hydrocarbons in flames, Proceedings of the Combustion Institute, 35, 1735-1743, 10.1016/j.proci.2014.06.137, 2015.

van der Werf, G. R., Randerson, J. T., Giglio, L., van Leeuwen, T. T., Chen, Y., Rogers, B. M., Mu, M. Q., van Marle, M. J. E., Morton, D. C., Collatz, G. J., Yokelson, R. J., and Kasibhatla, P. S.: Global fire emissions estimates during 1997-2016, Earth System Science Data, 9, 697-720, 10.5194/essd-9-697-2017, 2017.

Wang, H.: Formation of nascent soot and other condensed-phase materials in flames, Proceedings of the Combustion Institute, 33, 41-67, 10.1016/j.proci.2010.09.009, 2011.

Wang, H., Guan, J. W., Xu, G. X., Mercier, X., Zhang, J. Y., Guo, H. T., Yu, T. Z., Gui, H. Q., Huang, T., Truhlar, D. G., and Wang, Z. D.: Resonance-stabilized radical clustering bridges the gap between gaseous precursors and soot in the inception stage, Proc. Natl. Acad. Sci. U. S. A., 122, 10.1073/pnas.2503292122, 2025.

Wang, J. H., Jiang, H. X., Chen, Y. J., Han, Y., Cai, J. J., Peng, Y., and Feng, Y. L.: Emission characteristics and influencing mechanisms of PAHs and EC from the combustion of three components (cellulose, hemicellulose, lignin) of biomasses, Sci. Total Environ., 859, 10.1016/j.scitotenv.2022.160359, 2023.

Xu, L., Wang, Y., and Liu, D.: Effects of oxygenated biofuel additives on soot formation: A comprehensive review of laboratory-scale studies, Fuel, 313, 10.1016/j.fuel.2021.122635, 2022.

Zhang, G. H., Peng, X. C., Song, W., Huang, X. R., Li, Y. T., Chen, B. Y., Song, J. Z., Wang, X. M., and Bi, X. H.: Single-particle insights into the initial mixing state of black carbon and polycyclic aromatic hydrocarbons from biomass and coal combustion, Atmos. Environ., 374, 10.1016/j.atmosenv.2026.121963, 2026.

Zhang, X., Liu, H., Cheng, J., Song, W., Wang, H., Zhang, Y., and Wang, X.: Gas-Phase Oxidation of Guaiacol by NO3 Radicals: Kinetic Measurements and Implications, ACS ES&T Air, 2, 903-910, 10.1021/acsestair.4c00353, 2025.

Zhao, X., Yang, F. X., Li, Z. H., and Tan, H. Z.: Formation and emission characteristics of PAHs during pyrolysis and combustion of coal and biomass, Fuel, 378, 10.1016/j.fuel.2024.132935, 2024.

https://doi.org/10.5194/egusphere-2026-5314
Preprint. Discussion started: 28 September 2026


Zhu, X. M., Han, Y., Feng, Y. L., Cheng, P. H., Peng, Y., Wang, J. H., Cai, J. J., and Chen, Y. J.: Formation and
490 emission characteristics of intermediate volatile organic compounds (IVOCs) from the combustion of biomass and their cellulose, hemicellulose, and lignin, Atmos. Environ., 286, 10.1016/j.atmosenv.2022.119217, 2022.